Applied Physics Letters

Raman frequencies of diamond under non-hydrostatic pressure

Cite as: Appl. Phys. Lett. **119**, 211902 (2021); https://doi.org/10.1063/5.0069818
Submitted: 02 September 2021 • Accepted: 04 November 2021 • Published Online: 22 November 2021

Alaa Mohammed Idris Bakhit, S. Mutisya and S. Scandolo

Applied Physics Letters ARTICLE scitation.org/journal/apl

Raman frequencies of diamond under non-hydrostatic pressure

Cite as: Appl. Phys. Lett. **119**, 211902 (2021); doi: 10.1063/5.0069818
Submitted: 2 September 2021 · Accepted: 4 November 2021 ·
Published Online: 22 November 2021

Alaa Mohammed Idris Bakhit,[1,2,a)] S. Mutisya,[3] and S. Scandolo[4]

AFFILIATIONS

[1]The ICTP East African Institute for Fundamental Research (EAIFR), University of Rwanda, Kigali, Rwanda
[2]Centro de Física de Materiales CSIC/UPV-EHU-Materials Physics Center, E-20018 San Sebastían, Spain
[3]SUBATECH (IMT-Atlantique, CNRS-IN2P3, Université de Nantes), 44307 Nantes, France
[4]The Abdus Salam International Centre for Theoretical Physics (ICTP), Strada Costiera 11, I-34151 Trieste, Italy

[a)]Author to whom correspondence should be addressed: alaa.mohammed@ehu.eus

ABSTRACT

The Raman frequencies of diamond subjected to non-hydrostatic uniaxial stress along the [001] and [111] crystallographic axes have been calculated with density-functional-theory methods and the results fitted to a simple analytical form. The data are analyzed in the context of the recently proposed use of the shift of the high-frequency edge of the Raman band of diamond as a pressure scale in diamond-anvil cell experiments. Combining theoretical and experimental data, we are able to determine the stress state of the diamond anvil in ultra-high-pressure experiments. We find that shear stresses close to the tip of the anvil can reach values exceeding 1 Mbar.

Advances in the design and assembly of diamond anvil cells are pushing the boundaries of static high-pressure experiments to multi-megabar pressures.[1] Accurate determinations of pressure at these conditions are challenging.[2] Commonly used methods include the pressure-dependence of the ruby fluorescence lines and the pressure-induced shift of the x-ray diffraction peaks of pressure standards, such as noble metals. In a recent experiment,[3] the pressure–volume relation for Au and Pt was calibrated up to 1 TPa (10 Mbar) but other pressure standards are calibrated at lower pressures, and fluorescence signals are difficult to extract at multimegabar pressures. An alternative method to determine pressure in multimegabar experiments has emerged in the last few years, based on the shift of the high-frequency edge of the Raman band of diamond.[4–13]

In the standard geometry of high-pressure experiments with diamond anvil cells (see Fig. 1), optical measurements, including Raman spectroscopy, are carried out by aligning a laser beam parallel to the principal axis of the diamond anvil, which normally coincides with the [001] crystallographic axis, or more rarely with the [111] axis. Before entering the sample chamber, the laser beam traverses the entire diamond anvil from the loading face to the culet, and in doing so, it probes diamond at different strain states, from the virtually unstrained state close to the loading face, to the state of maximum strain (and pressure) close to the diamond anvil culet. The Raman signal scattered from the continuum of diamond strain states probed by the beam gives rise to a band extending from 1330 cm^{-1}, the ambient-pressure value of the diamond Raman frequency, to a maximum frequency that depends on the maximum strain reached at, or close to, the culet. Under the assumption that the strain state corresponding to the high-frequency Raman edge is determined uniquely by the pressure measured in the sample and is not influenced by the size, shape, and crystal orientation of the diamond anvil, the method is, in principle, a simple and noninvasive scheme for pressure determination at multimegabar pressures.

Originally proposed by Syassen and Hanfland,[4] who measured the Raman edge of a diamond cell up to 30 GPa, the method has been refined and calibrated by a number of authors in the last decades.[6–13] The calibration was extended in Ref. 13 to 400 GPa and is routinely used in multimegabar experiments.[14,15]

The reliability of the method is, however, subject to the verification that a single universal calibration is sufficient to describe the dependence of the high-frequency Raman edge on the pressure in the sample. Evidence suggests for example that different diamond crystallographic orientations[7] lead to qualitatively different calibration curves.

Central to any quantitative assessment of the Raman edge as a pressure determination method are two important, but loosely

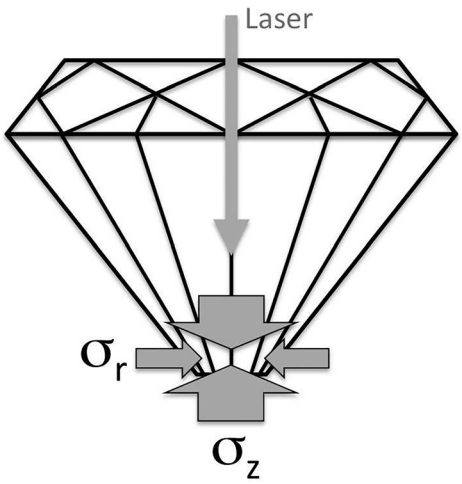

FIG. 1. Laser beam alignment and typical stress configuration close to the culet of the diamond in a diamond-anvil cell.

characterized properties of the diamond anvil: (i) the stress/strain field distribution inside the anvil, in particular, close to the culet, and (ii) the behavior of the Raman frequency peaks of diamond as a function of non-hydrostatic strain. The former is known to depend on the size, shape, crystal orientation of the diamond anvil, and finite-element calculations suggest that the state of maximum stress is achieved along the principal axis, close to the diamond tip.[16]

On the other hand, the behavior and splitting of the diamond Raman peaks under non-hydrostatic conditions has been measured to Mbar pressures only for loading along the [111] crystallographic axis.[7] For the most commonly employed orientation of the diamond anvil, corresponding to loading along [100], data are available only up to 1 GPa,[4] due to symmetry constraints. Stress field and Raman peak splitting are intimately connected: If the stress field inside the diamond anvil was known, measurements of the Raman edge could in principle be used to determine the Raman frequency of diamond under non-hydrostatic stresses. Vice versa, if the Raman frequency was known as a function of arbitrary strains, measurements could be used in principle to determine the stress state of the anvil. In Ref. 7, the state stress of the diamond anvil subjected to loading along [111] was extracted from the measurement of the splitting of the Raman peak, under the assumption of a linear dependence of the splitting vs the shear stress and also under the assumption that the stress component along the loading axis is equal to the pressure in the sample. As we will see later on, these assumptions, especially the first one, are justified only for compression along [111] and not along [100].

The purpose of this work is to facilitate and improve the interpretation of Raman-edge measurements by providing accurate theoretical values for the Raman frequencies of diamond as a function of stress under non-hydrostatic loading along the [111] and [001] axes, using first-principle, density-functional-theory (DFT) methods.

Calculations were performed within DFT, the pseudopotential approximation, and with a plane wave expansion of the wave functions, as implemented in the Quantum-Espresso code.[17,18] Different choices of the pseudopotential (norm-conserving and ultrasoft) and of the exchange-correlation functional (local-density approximation or gradient-corrected functional[19]) were tested (see the supplementary material) against available experimental data for hydrostatic compression.[12] The best agreement with hydrostatic experimental data was obtained with a norm-conserving pseudopotential and with the local-density approximation, see Figs. 2 and S1 in the supplementary material. All calculations reported below were performed with these approximations.

Calculations under loading along the [111] and [001] axes were performed using rhombohedral or body-centered tetragonal unit cells, respectively (see the supplementary material). In both cases, we denote by σ_z the stress along the loading axis and by σ_r the stress in the perpendicular direction.

Under both types of loading the triply degenerate diamond Raman frequency splits into a doublet (ω^d) and a singlet (ω^s).[4] Calculations of $\omega^{(d,s)}$ on a large grid of values of $\sigma_{r,z}$ (see Figs. S2 and S3 in the supplementary material) were fitted to a polynomial form of the type

$$\begin{aligned}\omega(\sigma_r,\sigma_z) = \omega_H(\sigma_{AV}) - (a_0 + a_1(\sigma_{AV} - 300) \\ + a_2(\sigma_{AV} - 300)^2)\tau - (b_0 + b_1(\sigma_{AV} - 300) \\ + b_2(\sigma_{AV} - 300)^2)\tau^2 - (c_0 + c_1(\sigma_{AV} - 300) \\ + c_2(\sigma_{AV} - 300)^2)\tau^3, \end{aligned} \quad (1)$$

where $\sigma_{AV} = (\sigma_z + 2\sigma_r)/3$ (in GPa), $\tau = \sigma_z - \sigma_r$, and $\omega_H(\sigma_{AV}) = \omega_\circ + a\sigma_{AV} + b\sigma_{AV}^2$. In terms of σ_z and σ_r, the grid points were uniformly distributed in the domain $100 < \sigma_{AV} < 400$ GPa and $0 \leq \tau \lesssim 130$ GPa. Notice that we are assuming that $\sigma_z \geq \sigma_r$. The twelve parameters reported in Table I gave the best fit to the calculated data. The small disagreement between the parameters of $\omega_H(\sigma_{AV})$ for [111] and [001] has a negligible effect for $\tau = 0$ but improves the quality of the fit for $\tau \neq 0$. The standard deviation between the *ab initio* data and form (1) is about 10 cm^{-1}.

Figure 3 shows how the singlet and the doublet split as a function of the shear stress τ, for different values of σ_{AV}. The linear coefficient of the singlet-doublet splitting at small τ is much larger along [111] than [001]. This is consistent with ambient pressure data.[4] The coefficients measured at ambient pressure are 2.2 and 0.73 cm^{-1}/GPa for

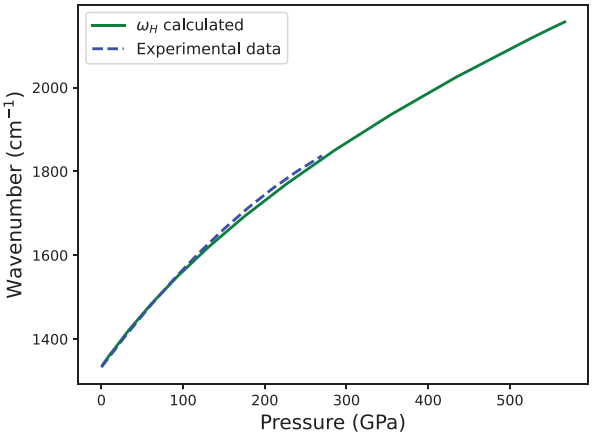

FIG. 2. Raman frequency of diamond under hydrostatic compression. Comparison between experimental data[12] and our *ab initio* calculations.

TABLE I. Parameters of the fit of the singlet and doublet Raman frequencies to the polynomial in Eq. (1).

Parameter	$\omega^{(d)}_{[001]}$ fit	$\omega^{(s)}_{[001]}$ fit	$\omega^{(s)}_{[111]}$ fit	$\omega^{(d)}_{[111]}$ fit
ω_0	1364.423 069	1364.423 069	1344.423 069	1344.423 069
a	2.438 42	2.453 32	2.280 08	2.282 48
b	−0.002 167 28	−0.002 240 11	−0.00174805	−0.001 752 77
a_0	−0.016 616 9	−0.079 006 6	−1.0498	0.536 349
a_1	0.001 546 63	0.001 157 92	0.000 926 507	−0.000 587 159
a_2	$1.011\,48 \times 10^{-5}$	$1.706\,04 \times 10^{-5}$	$-3.612\,38 \times 10^{-6}$	$-3.914\,98 \times 10^{-7}$
b_0	0.000 661 298	0.000 304 746	0.000 152 316	0.000 466 838
b_1	$-1.893\,95 \times 10^{-5}$	$-2.477\,92 \times 10^{-5}$	$-1.621\,23 \times 10^{-6}$	$-2.574\,06 \times 10^{-6}$
b_2	$-9.574\,08 \times 10^{-8}$	$-1.098\,79 \times 10^{-7}$	$-2.235\,98 \times 10^{-8}$	$-1.882\,92 \times 10^{-8}$
c_0	$5.751\,32 \times 10^{-6}$	$8.172\,74 \times 10^{-6}$	$-3.236\,69 \times 10^{-7}$	$-2.232\,24 \times 10^{-7}$
c_1	$4.469\,75 \times 10^{-8}$	$4.680\,57 \times 10^{-8}$	$4.243\,24 \times 10^{-9}$	$3.246\,83 \times 10^{-9}$
c_2	$5.250\,55 \times 10^{-11}$	4.53604×10^{-11}	$7.095\,76 \times 10^{-11}$	6.3714×10^{-11}

[111] and [001], respectively.[4] These compare well with our estimates of 2.3 and 0.68 cm^{-1}/GPa for [111] and [001], respectively, obtained by extrapolating formula 1 to ambient pressure [notwithstanding the fact that ambient pressure is well outside the range where Eq. (1) was fitted]. While the linear behavior extends to large τ in the case of [111], higher order terms become significant already at small τ in the case of [001], also as a consequence of the smaller value of the linear coefficient. Notice that the maximum shear stresses reported in the literature are 80 GPa for [111] loading and 100 GPa for [110] loading.[9]

We are now in a position to extract information about the stress states in the diamond anvil based on a comparison between experimental data and calculations. We begin by remarking that in Eq. (1), the values of $\omega^{(d)}$ and $\omega^{(s)}$ are expressed as analytical functions of σ_{AV} and τ. As a consequence, Eq. (1) can be inverted to yield the values of σ_{AV} and τ corresponding to a given pair of values for $\omega^{(d)}$ and $\omega^{(s)}$. Therefore, in a situation where both $\omega^{(d)}$ and $\omega^{(s)}$ are known from experiments, the stress state (σ_{AV},τ) of the diamond anvil can be extracted by inverting Eq. (1).

In the case of loading along [111], singlet and doublet frequencies have been measured as a function of the pressure in the sample (P_s) in Ref. 7. Using the values of Ref. 7 for $\omega^{(d)}$ and $\omega^{(s)}$, we inverted Eq. (1) to extract the values of σ_{AV} and τ corresponding the specific stress state of the diamond anvil in the experiment of Ref. 7. The results (Fig. 4) show that shear stress grows almost linearly with the sample pressure and reaches values as high as ∼70 GPa at $P_s = 220$ GPa. The results also show that the sample pressure is well approximated by σ_z, the stress component along the loading axis. On the contrary, the stress component parallel to the culet surface is about half of the vertical component. In Ref. 7, the stress state of the anvil was determined starting from the measurement of $\omega^{(d)}$ and $\omega^{(s)}$ by making two crucial assumptions: (i) the splitting of the Raman peaks depends linearly on the shear stress, and (ii) the value of σ_z coincides with the pressure in the sample. Our independent analysis of the experimental data confirms that the two assumptions are indeed correct. In fact, (i) the calculated splittings for [111] (left panel of Fig. 3) behave linearly with the shear stress, and (ii) the calculated value of σ_z turns out to be fairly close to the sample pressure (Fig. 4).

In the case of loading along [001], only the singlet is observed in the diamond-anvil cell geometry, due to selection rules.[4] As a consequence, it is impossible to invert Eq. (1) and obtain the stress state directly from the Raman data. In order to invert Eq. (1), we are, therefore, forced to introduce an additional constraint. We follow the indications of Ref. 16 and assume that σ_z equals the sample pressure P_s. Incidentally, this is consistent also with our findings for loading along [111], as described above. Under this assumption, we consider the Raman data reported in Ref. 13 for ω_S and invert Eq. (1) to obtain the

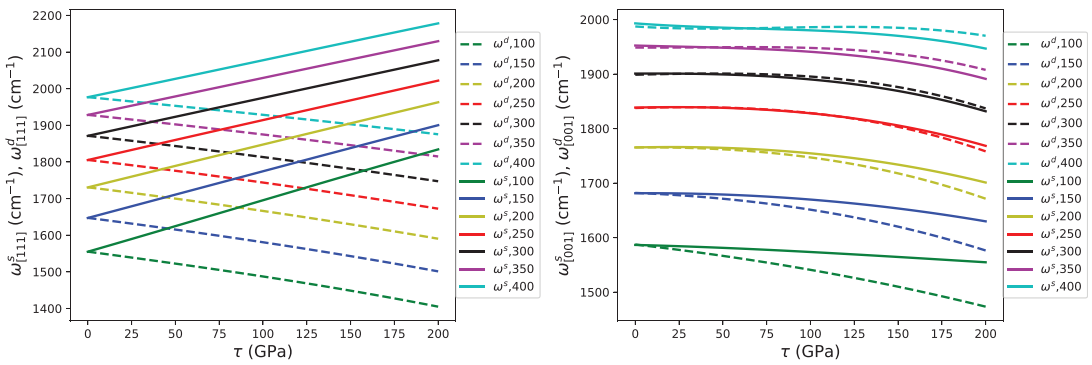

FIG. 3. Frequencies of the Raman singlet and doublet as function of τ at fixed values of the pressure σ_{AV}. Left: [111] loading; right: [001] loading.

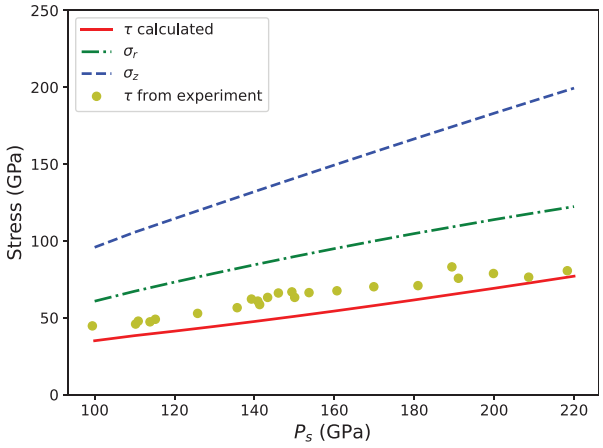

FIG. 4. Calculated values of the stress along the loading axis (σ_z) and along the radial direction (σ_r), and shear stress τ, as a function of the pressure P_s in the sample, for diamond-anvil cell loaded along the [111] diamond axis. The experimental data for the shear stress τ reported in Ref. 7 are also shown. Notice that our definition of τ ($\tau = \sigma_z - \sigma_r$) differs by a factor of two with respect to the definition employed in Ref. 7, where $\tau = (\sigma_z - \sigma_r)/2$.

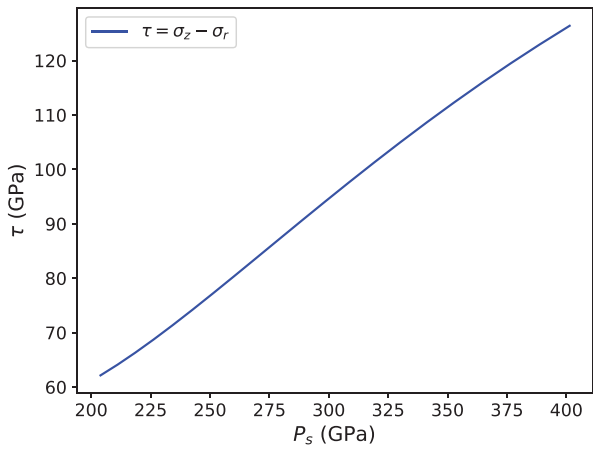

FIG. 5. Shear stress τ as a function of the sample pressure, for diamond-anvil cell loaded along the [001] diamond axis, under the assumption that the stress component along the loading axis (σ_z) coincides with the pressure in the sample P_s.

shear stress in the anvil as a function of the pressure in the sample. The results, shown in Fig. 5, indicate that the shear stress grows with the sample pressure and reaches a value of about 125 GPa at the highest sample pressure reported in Akahama's [001] experiment (401 GPa).

The maximum shear stress determined in this work for diamond-anvil loading along [111] and [001] is large but at least in the case of [001], they are still considerably below the theoretical limit for the onset of an elastic instability ($\tau_{max} = 200$ GPa) for uniaxial compression along the cubic axis.[20] However, an extrapolation of the data shown in Fig. 5 indicates a theoretical limit $P_s \sim 600$ GPa for the maximum pressure achievable with diamond anvil cells in the standard geometry used in the experiments of Refs. 7 and 13.

See the supplementary material for details about the convergence tests and constant volumes calculations. Also, the input files are included.

AUTHOR DECLARATIONS

Conflict of Interest

The authors have no conflicts to disclose.

DATA AVAILABILITY

The data that support the findings of this study are openly available in GitHub, Ref. 21.

REFERENCES

[1]M. McMahon, Nat. Mater. **17**, 858–859 (2018).
[2]R. Jeanloz, Science **372**, 1037–1038 (2021).
[3]D. Fratanduono, M. Millot, D. Braun, S. Ali, A. Fernandez-Pañella, C. Seagle, J.-P. Davis, J. Brown, Y. Akahama, R. Kraus *et al.*, Science **372**, 1063–1068 (2021).
[4]M. Hanfland and K. Syassen, J. Appl. Phys. **57**, 2752 (1985).
[5]R. D. Markwell and I. S. Butler, Can. J. Chem. **73**, 1019–1022 (1995).
[6]Y. Akahama and H. Kawamura, J. Appl. Phys. **96**, 3748 (2004).
[7]Y. Akahama and H. Kawamura, J. Appl. Phys. **98**, 083523 (2005).
[8]Y. Akahama and H. Kawamura, J. Appl. Phys. **100**, 043516 (2006).
[9]Y. Akahama and H. Kawamura, High Pressure Res. **27**, 473 (2007).
[10]B. J. Baer, M. E. Chang, and W. J. Evans, J. Appl. Phys. **104**, 034504 (2008).
[11]L. Sun, A. L. Ruoff, and G. Stupian, Appl. Phys. Lett. **86**, 014103 (2005).
[12]N. Dubrovinskaia, L. Dubrovinsky, R. Caracas, and M. Hanfland, Appl. Phys. Lett. **97**, 251903 (2010).
[13]Y. Akahama and H. Kawamura, J. Phys.: Conf. Ser. **215**, 012195 (2010).
[14]R. P. Dias and I. F. Silvera, Science **355**, 715–718 (2017).
[15]R. Helled, G. Mazzola, and R. Redmer, Nat. Rev. Phys. **2**, 562–574 (2020).
[16]S. Merkel, R. J. Hemley, and H-k Mao, Appl. Phys. Lett. **74**, 656–658 (1999).
[17]P. Giannozzi, S. Baroni, N. Bonini, M. Calandra, R. Car, C. Cavazzoni, D. Ceresoli, G. L. Chiarotti, M. Cococcioni, I. Dabo *et al.*, "Quantum espresso: A modular and open-source software project for quantum simulations of materials," J. Phys.: Condens. Matter **21**, 395502 (2009).
[18]P. Giannozzi, O. Andreussi, T. Brumme, O. Bunau, M. B. Nardelli, M. Calandra, R. Car, C. Cavazzoni, D. Ceresoli, M. Cococcioni *et al.*, "Advanced capabilities for materials modelling with quantum espresso," J. Phys.: Condens. Matter **29**, 465901 (2017).
[19]J. P. Perdew, K. Burke, and M. Ernzerhof, Phys. Rev. Lett. **77**, 3865–3868 (1996).
[20]J. Zhao, S. Scandolo, J. Kohanoff, G. L. Chiarotti, and E. Tosatti, Appl. Phys. Lett. **75**, 487 (1999).
[21]M. Alaa Mohammed Idris Bakhit and S. Scandolo (2021). "Supporting information on Raman frequencies of diamond under non hydrostatic pressure," GuiHub. https://github.com/AlaaMIB2325/Supporting-information-on-Raman-frequencies-of-diamond-under-non-hydrostatic-pressure